JMEPEG (2002) 11:51-63

Material Flow and Microstructure in the Friction Stir Butt Welds of the Same and Dissimilar Aluminum Alloys

J.H. Ouyang and R. Kovacevic

(Submitted 21 May 2001; in revised form 8 July 2001)

The material flow and microstructural evolution in the friction stir welds of a 6061-Al alloy to itself and of a 6061-Al alloy to 2024-Al alloy plates of 12.7 mm in thickness were studied under different welding conditions. The results showed that plastic deformation, flow, and mechanical mixing of the material exhibit distinct asymmetry characteristics at both sides of the same and dissimilar welds. The microstructure in dissimilar 6061-Al/2024-Al welds is significantly different from that in the welds of a 6061-Al alloy to itself. Vortex-like structures featured by the concentric flow lines for a weld of 6061-Al alloy to itself, and alternative lamellae with different alloy constituents for a weld of 6061-Al to 2024-Al alloy, are attributed to the stirring action of the threaded tool, in situ extrusion, and traverse motion along the welding direction. The mutual mixing in the dissimilar metal welds is intimate and far from complete. However, the bonding between the two Al-alloys is clearly complete. Three different regions in the nugget zone of dissimilar 6061-Al/2024-Al welds are classified by the mechanically mixed region (MMR) characterized by the relatively dispersed particles of different alloy constituents, the stirring-induced plastic flow region (SPFR) consisting of alternative vortex-like lamellae of the two Al-alloys, and the unmixed region (UMR) consisting of fine equiaxed grains of the 6061-Al alloy. Within all of these three regions, the material is able to withstand a very high degree of plastic deformation due to the presence of dynamic recovery or recrystallization of the microstructure. The degree of material mixing, the thickness of the deformed Al-alloy lamellae, and the material flow patterns depend on the related positions in the nugget zone and the processing parameters. Distinct fluctuations of hardness are found to correspond to the microstructural changes throughout the nugget zone of dissimilar welds.

Keywords dissimilar Al-alloy joining, friction stir welding, material flow, microstructure

1. Introduction

Friction stir welding (FSW) has recently caught great attention of the welding community for fabricating high-quality butt and lap joints of aluminum alloys.[1-5] It has proven to produce excellent results with good repeatability in bending, tensile, and fatigue endurance tests for various manufacturing industries, especially in aerospace and shipbuilding.[4-9] To date, most research has concentrated on developing the tools and procedures for making reliable welds and on characterizing the properties of welds.[2-11] However, very little is known about the material flow behavior during FSW. Techniques of steel shot tracer and sudden-stop action of the stirring tool were used to study the flow of material in the welds.[2] Based on the measured results in welds of the 6061-Al alloy, the material movement within welds is considered to be by either simple extrusion or chaotic mixing, depending on where the material originates within the weld zone.[2] It is perceived that a process model could yield more information on material mixing, defect presence, and retained oxide films.[12,13] However, the difficulties in predicting material flow behavior are mainly due to the lack of detailed material characteristic information such as the viscous coefficient and other thermal physical properties at elevated temperatures.

Although very few studies have been undertaken successfully for the FSW of dissimilar Al-alloys, it is evident that the microstructural evolution and material flow behavior in the dissimilar welds are quite complex.[3-7,14-19] The FSW of a wide variety of both the same and dissimilar Al-alloys to one another has been shown to involve dynamic recrystallization as the mechanism to accommodate the superplastic deformation that facilitates the bond.[14-19] Dissimilar welds of a 5083 aluminum to a 6082 aluminum[3] showed that a material with a lower strength should be placed at the advancing side and generally, a higher welding speed and a consumable strip with a lower strength is preferred. Aluminum strip consumable inserts were used to compensate for a lack of material. Dissimilar metal plates (6 mm thick) of copper to a 6061-Al alloy, and a 2024-Al alloy to a 6061-Al alloy were friction-stir welded at various welding parameters.[14-16,19] It should be noted that even under the optimized conditions, no good welds of perfect quality were obtained for these alloy systems. All of the obtained welds were with an unwelded seam, large open (void) zones, and oxide inclusions at the root of plates. The welds produce variations of vortex and other swirl-like intercalations characterized by dynamic recrystallization and limited grain growth. For the 6061-Al/Cu system, there does not seem to be a significant effect on the weld microstructure when the tool rotational speed is varied from 400 to 1200 rpm. However, there is a recognizable effect of the rotational speed on the residual grain size in the weld zone for the 6061-Al/2024-Al welds.

J.H. Ouyang and **R. Kovacevic,** Research Center for Advanced Manufacturing, Department of Mechanical Engineering, Southern Methodist University, 1500 International Parkway, Suite 100, Richardson, TX 75081. Contact e-mail: kovacevi@seas.smu.edu.

Despite extensive scientific interest in the FSW of dissimilar metals, no systematic study on the characterization of the material flow behavior and the effects of welding parameters on the microstructure and properties of dissimilar welds on thick Al-alloy plates appear to be available in the open literature. In this article, a feasibility study of FSW on the same and dissimilar Al-alloy plates as thick as 12.7 mm was performed by using a specially designed tool. The welding parameters are discussed to understand how these aspects affect the flow and mixing of material in the welds and thereby the microstructure formation.

2. Experimental Procedure

The experimental setup consists of a vertical milling machine, two rotary acoustic emission (AE) sensors with an amplifier, and a data acquisition system based on a PC, an infrared camera with an image capturing board, a specially designed tool, rigid fixturing, and samples for butt welding, as shown in Fig. 1(a). All the welds are made in a butt-weld configuration. Figure 1(b) shows the configuration of sensors and different Al-alloy plates for the same and dissimilar metal welds. For detecting the AE signals from the FSW process, two rotary AE

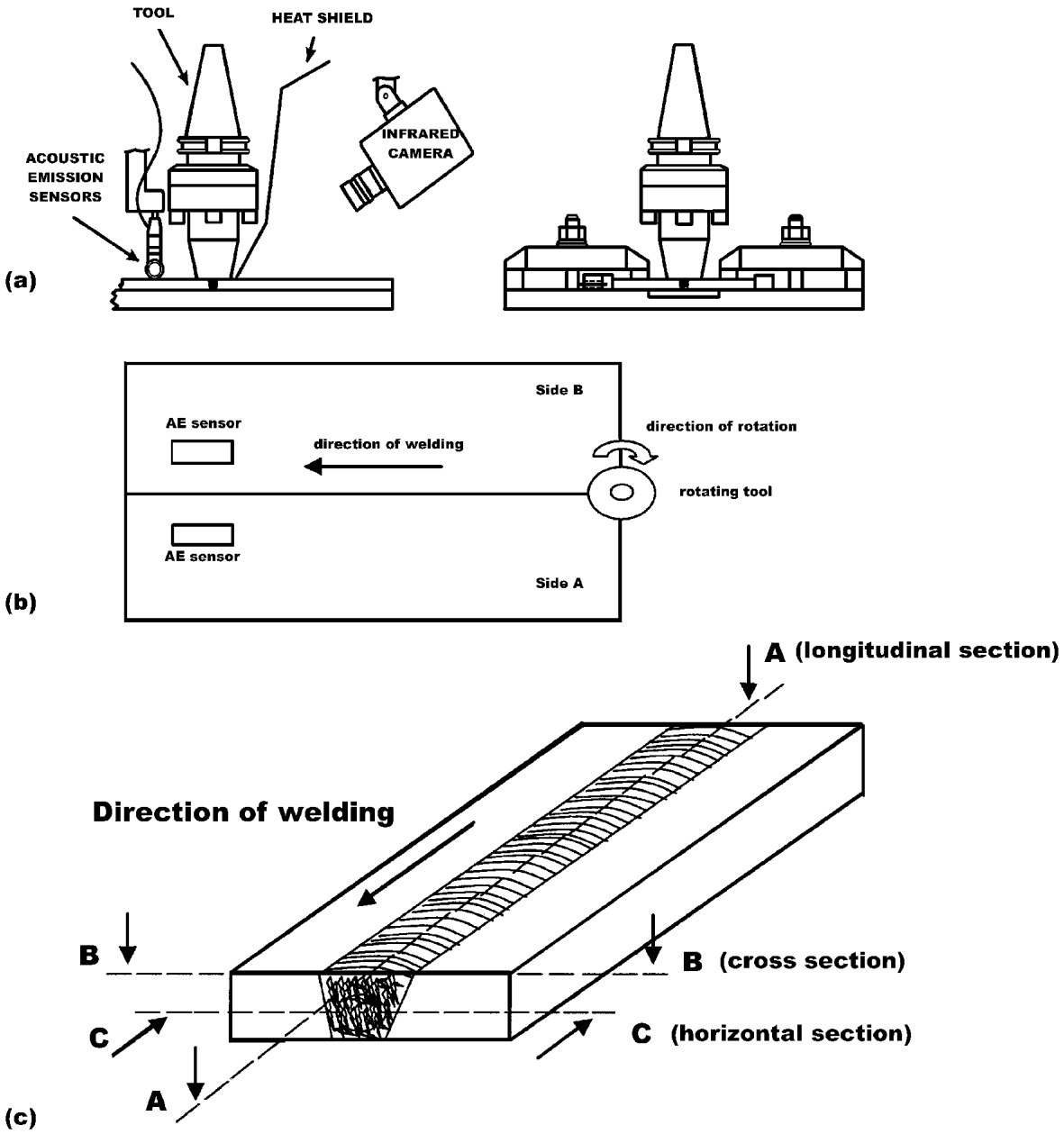

Fig. 1 Experimental set up and weld configuration: (a) experimental set-up; (b) schematic diagram showing the configuration of sensors and different Al-alloy plates (Side A = 6061-Al or 2024-Al alloy plate, and Side B = 6061-Al alloy plate for the same or dissimilar metal welds); (c) schematic diagram showing the positions of samples taken from different sections of the welds (B—B, cross section; A—A, longitudinal section; C—C, horizontal section)

sensors are fixed symmetrically with respect to the weld centerline. The contact points of the rotary AE sensors with the workpiece are located 30 mm from the weld centerline and in front of the tool. The material used for the tool shoulder is a typical tool steel. The tool pin material is a tool steel grade with a good balance of abrasive resistance, strength, and fracture toughness. The 6061-T6 Al-alloy plate is 12.7 mm in thickness with a chemical composition of (wt.%) 0.8-1.2 Mg, 0.4-0.8 Si, 0.7 Fe, 0.15-0.4 Cu, 0.15 Mn, 0.04-0.35 Cr, 0.25 Zn, and 0.15 Ti. The 2024-T3 Al-alloy plate is the same thickness and with a chemical composition of (wt.%) 3.8-4.9 Cu, 1.2-1.8 Mg, 0.3-0.9 Mn, 0.4 Fe, 0.4 Si, and 0.2 Zn. A number of FSW experiments for the 6061-Al alloy to itself, and for the 6061-Al alloy to 2024-Al alloy are carried out to obtain the optimum parameters by adjusting the rotational speed of the tool and the welding speed. The welding parameters are as follows: 151-914 rpm for the rotational speed and 57-330 mm/min for the welding speed. Other conditions, including the threaded geometry and plunge depth of the stir tool, are kept constant.

For microstructural analyses, the welds are sectioned longitudinally, horizontally, and cross-sectionally, respectively, as shown in Fig. 1(c) and then are prepared by using standard metallographic procedures. The samples are etched by using a modified Kellers' reagent. Observations of plastic deformation, material flow, and microstructures are performed by using a high-resolution optical microscope. Vickers microhardness measurements are performed on both the cross and longitudinal sections of the welds by using a microhardness tester at a 200 g load and a 15 s dwell time.

3. Results and Discussion

3.1 Material Flow and Microstructure in a Weld of the 6061-Al Alloy to Itself

Figure 2 shows the typical features of all different zones in a weld cross section (B—B) of the 6061-Al alloy to itself under the welding condition of 416 rpm for the rotational speed and 133 mm/min for the welding speed. The positions A-F marked in Fig. 2(a) are located in a different microstructural zone. The micrographs shown in Fig. 2 show that the microstructure of the weld is complex and highly dependent on the position within the welded zone. This result arises because of the large local variations in the plastic flow and the thermal history that results from the interaction with the tool. The characteristic annular-banded structure is distinctly observed to be asymmetric and more obvious on the right side of the weld as shown in Fig. 2(a). A severe deformation has also occurred along the top surface of the weld where the shoulder of the tool is in contact with the workpiece. The stirring action completely obliterates any remnants of the joint line. The flow lines shown in Fig. 2(b) are real and apparently represent plastic deformation increments that develop as the rotating tool moves through the joint. Although it is well known that in FSW, material is transported from the leading face to the retreating edge, it is only recently that Colligan[2] showed that with a threaded tool, material from the upper part of the parent plate is forced down into the weld, whereas material from the lower part of the parent plate is moved toward the top surface. Material may travel several times around the tool, dependent on the rotational speed of the tool before being redeposited. There is little flow of material in the area near the bottom of the weld.

The microstructure in the stir zone is characterized by a fine grain size occurring in a discrete series of bands and some precipitate mainly distributed at the grain boundaries as shown in Fig. 2(c). There is also still some debate concerning the origin of the annular rings observed within the nugget zone that in one study have been attributed to an abrupt variation in the grain size and precipitate density. The fine equiaxed grains in the nugget zone suggest effective strains together with a microstructural evolution that occurs by a combination of hot working and a dynamic recovery or recrystallization. The distinct boundary on either side of the nugget zone clearly delineates where a fully recrystallized microstructure ends and a partially recrystallized structure starts as shown in Fig. 2(d). The temperature reached in the nugget zone is known to be in the range of 450-500 °C, and the thermomechanically affected zone (TMAZ) is in the range of 350-450 °C for the 6061-Al alloy.[16] From Fig. 2(e), more distinct precipitates and coarsened grains are observed at the deformed regions of the TMAZ in contrast with those in the nugget zone. The grains in the heat affected zone (HAZ) are severely coarsened by the FSW process shown in Fig. 2(f). The grains of the unaffected 6061-Al alloy are elongated along the rolled direction as shown in Fig. 2(g). The precipitates are mainly distributed at the interior of grains.

An analysis of longitudinal (A—A) and horizontal (C—C) sections in a weld of the 6061-Al alloy to itself is undertaken as shown in Fig. 3. Zigzag bonding is distinctly observed at the center of the nugget in Fig. 3(a) and (b). It is considered to be caused by the threaded tool. It suggests that although the bonding between the two plates is perfect, the mechanical mixing is far from complete in the nugget zone. A longitudinal section through the welds reveals the layered structures that may correspond to the onion rings. The nugget zone can be seen to consist of a number of horizontal layers. The top layer consists of horizontally striated material extending from the upper portion of the back edge of the pin, along the surface of the tool shoulder. This layered structure may be associated with differences in grain size and the precipitate distribution across the boundaries as shown in Fig. 3(c). The size of slightly elongated grains in the upper portion of Fig. 3(c) is clearly larger than that of equiaxed grains of the nugget zone shown in the lower portion. To some extent, the segregation of precipitate along the flow line occurs in the upper portion of Fig. 3. The zigzag bonding in the lower portion of the weld is also observed but much fainter. A distinct difference in grain size is observed across the interface between the nugget zone and the TMAZ from the horizontally section (C—C) at midthickness of the weld as shown in Fig. 3(d).

The configuration of the AE sensors used in this investigation allows us to pick up the AE signals from the same distance with respect to the place where acoustic emission is generated. Figure 4 shows the AE signals recorded at both sides A and B marked in Fig. 1(b) of the joint at 416 rpm for the rotational speed and 133 mm/min for the welding speed. The peak amplitudes of the AE signals from both sides that provide information of a structure while it is under stress are quite different. There is a strong relationship between the generated AE signals at the two sides of the joint and the plastic deformation mechan-

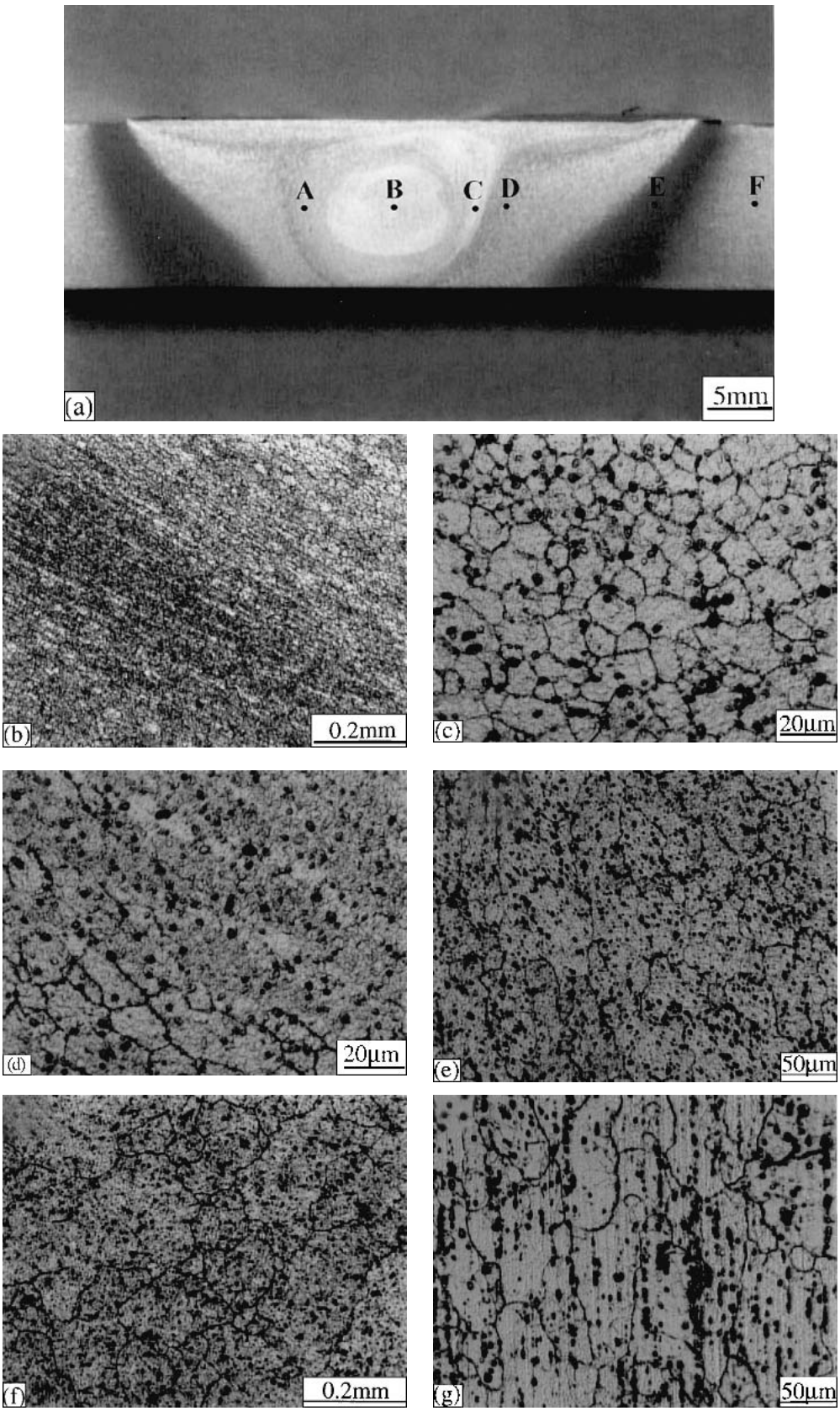

Fig. 2 Typical features of all different zones in a weld cross-section of 6061-Al alloy to itself at 416 rpm for rotational speed and 133 mm/min for welding speed: (a) weld cross section (B—B); (b) material flow patterns in the nugget zone around the position A; (c) equiaxed grains in the nugget zone around the position B; (d) interface transition between the equiaxed grains and flow line around the position C; (e) the TMAZ around the position D; (f) the HAZ around the position E; (g) unaffected 6061-Al alloy around the position F. Positions A–F are marked in (a).

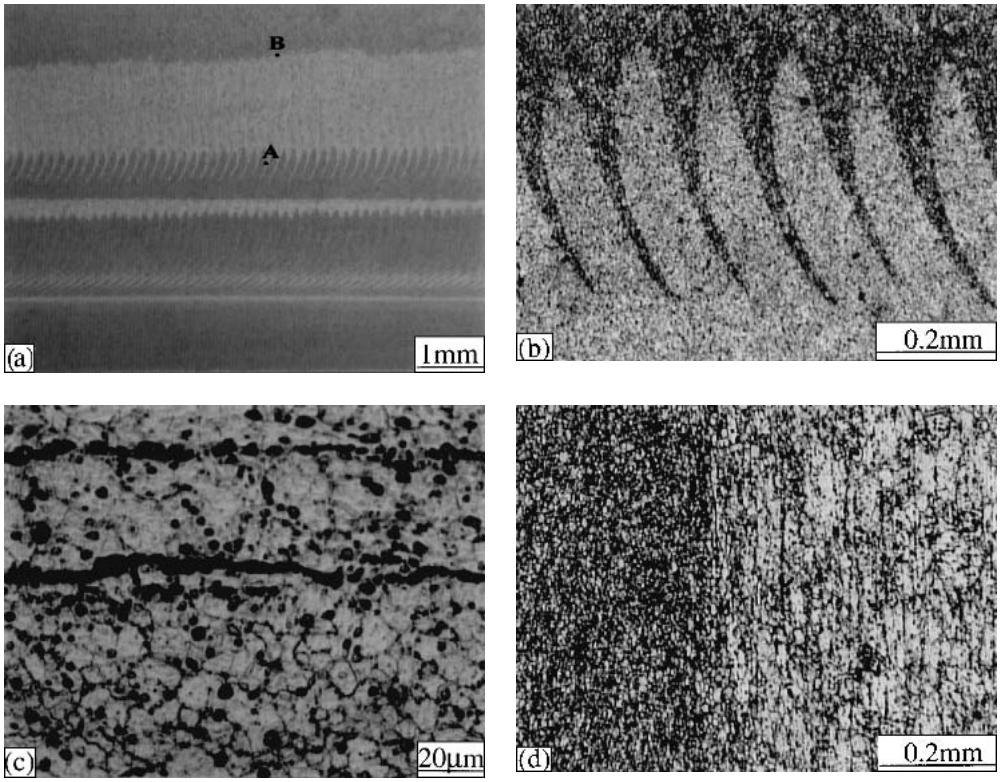

Fig. 3 Longitudinal and horizontal sections near the midthickness of a weld of 6061-Al alloy to itself at 416 rpm for rotational speed and 133 mm/min for welding speed: (a) weld longitudinal section (A—A); (b) zigzag bonding around the position A marked in (a); (c) micrograph showing the difference in grain size and precipitate distribution around the position B marked in (a) across the boundary of layered structure; (d) horizontal section (C—C) showing the transition between the nugget zone (left side) and the TMAZ (right side)

isms present during FSW. Most of the strain is caused by shear as material rotates around the tool during FSW. The sensor at side A detects a much stronger signal than that at side B. The number of AE events and the peak amplitude picked up from side A are found to be much higher than those recorded by the sensor placed at side B. Figure 4(c) shows the processed AE signals that are generated by the plastic deformation and flow of material. This result corresponds to the metallurgical observations of plastic deformation, flow of material, and microstructures as shown in Fig. 2.

3.2 Material Flow and Microstructure in a Dissimilar Metal Weld of 6061-Al Alloy to 2024-Al Alloy

Figure 5 shows the typical features of all different zones in a dissimilar weld cross section (B—B) of the 6061-Al alloy to 2024-Al alloy at 637 rpm for rotational speed and 133 mm/min for welding speed. The positions A-G marked in Fig. 5(a) are located in different microstructural zones. The asymmetric pattern of material flow is more clearly observed in the dissimilar weld in Fig. 5(a). The nugget zone shown in Fig. 5(a) is composed of different regions of intense plastic deformation and material flow of both Al-alloys. The morphology of the dissimilar 6061-Al/2024-Al weld is distinctly different from that of the 6061-Al alloy to itself. The vortex-like structure featured by the alternative lamellae of these two Al-alloys is attributed to the stirring action of the threaded tool, in situ extrusion, and traverse motion along the welding direction. The mutual mixing in the dissimilar metal welds is intimate and far from complete. However, the bonding between the two alloys is clearly complete (Fig. 5). Three different regions in the nugget zone of the dissimilar 6061-Al/2024-Al weld are classified by the mechanically mixed region (MMR) characterized by the dispersed particles of different alloy constituents in Fig. 5(c), the stirring-induced plastic flow region (SPFR) featured by the alternative vortex-like lamellae of two Al-alloys in Fig. 5(e), and the unmixed region (UMR) consisting of fine equiaxed grains of the 6061-Al alloy in Fig. 5(b). Within all of these three regions, the material is able to withstand the very high degree of plastic deformation due to the presence of a dynamic recovery or recrystallization of the microstructure. The degree of material mixing, the thickness of deformed Al-alloy lamellae, and the material flow patterns depend on the related position in the nugget zone as shown in Fig. 5 (b-h). At the upper portions of 2024-Al alloy side, the deformed grains at the TMAZ are perpendicular to the interface between the nugget zone and the TMAZ shown in Fig. 5(f), whereas at the lower portions of the 2024-Al alloy side, the deformed 2024-Al alloys at the TMAZ are parallel to the interface shown in Fig. 5(g). As the welding tool advances, these bands reveal a downward distortion of material. A severe plastic deformation of the 2024-Al alloy also occurs at the bottom of the nugget zone shown in Fig. 5(h).

The banded structure consisting of the alternative lamellae of 6061-Al and 2024-Al alloys becomes narrower in width of

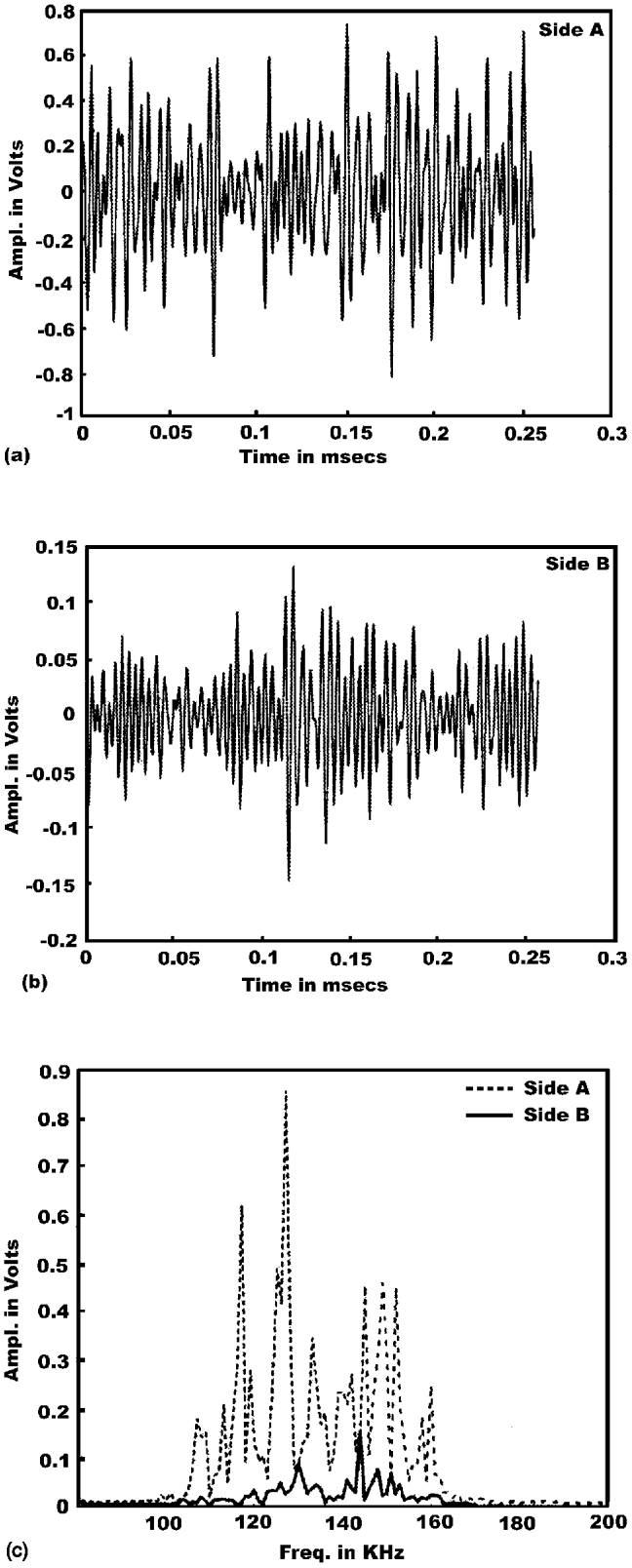

Fig. 4 Acoustic emission (AE) signals recorded at both sides of the weld of 6061-Al alloy to itself at 416 rpm for rotational speed and 133 mm/min for welding speed: (a) typical AE signals at the side A; (b) typical AE signals at the side B; (c) processed AE signals at both sides of the weld.

6061-Al lamellae with increasing distances from the center of the weld as shown in Fig. 5(e). The edge of all the lamellae is clearly delineated by an abrupt transition in the alloy constituents. The softened lamellae near the thread of the tool have been deformed as a viscous fluid of large viscosity. At the contact regions, the strain rate is controlled by the rotational speed. The strain rate must be of the order of 1000 s^{-1} or higher. It is obvious that FSW under such extreme conditions facilitates a severe plastic-flow behavior. The softened material is able to recover and behave like a liquid of high viscosity. Apart from the extreme strain rates at the MMR, the strain rate outside the contact section is also a function of the welding speed. This also gives rise to an extremely large strain rate gradient within the adjacent regions. In the SPFR, however, the stirring action of the threaded tool introduces distinct boundaries between alternative lamellae regions of these two alloys. The microstructure of the UMR in the nugget zone of the dissimilar welds is very similar to that of the same weld of the 6061-Al alloy to itself.

Figure 6 shows the typical morphology of longitudinal-(A—A) and horizontal-(C—C) sections of a dissimilar 6061-A1/2024-A1 weld. From Fig. 6(a), the dissimilar weld can be seen to consist of a number of horizontal layers. The top layer consists of a band of horizontally deformed 6061-Al alloy extending from the upper portion of the back edge of the tool along the surface of the tool shoulder. The alternative lamellae of these two Al-alloys are observed in the middle portion of the weld. The 6061-Al alloy at the subsurface layer is significantly propelled downward into the weld and is not chaotically scattered behind the tool. The material in this region appears to have been dragged behind the tool by the rotation of the threaded tool and is deposited in the nugget zone as alternative lamellae. These bands reveal a downward distortion of material that is much different from the flow pattern in a weld of the 6061-Al alloy to itself.

At the root of dissimilar welds, it appears that no mixing of material happens except the extensive plastic deformation of the 2024-A1 alloy. A distinct interface is observed between the nugget zone and the 2024-Al alloy at the root of the plate. In dissimilar welds, not all material influenced by the tool is actually stirred in the welding process. Figure 6(b) shows the microstructure across the transition interface around the position A marked in Fig. 6(a) at the subsurface layer. From the horizontal section shown in Fig. 6(c), the plastic deformation and material flow of different alloy constituents are clearly observed to be asymmetrical in the nugget zone. The mechanical stirring and material mixing is close to the 2024-Al alloy side. At the 6061-Al side, more material keeps unmixed. The thread of the tool is found to assist in ensuring that the plastically deformed material is fully delivered around the tool, resulting in a void-free weld. The horizontal section also shows the distinctly different patterns of material flow at the beginning of the weld as contrasted to the steady weld as shown in Fig. 6(c-e). Material may travel many cycles around the tool before being redeposited at the beginning of the weld. A more complete mixing of material is clearly observed at the beginning of the weld due to the long-time rotation of the tool before the tool begins to traverse along the welding direction. Furthermore, as the rotational time becomes longer during the plungement of the tool, the mechanical mixing becomes

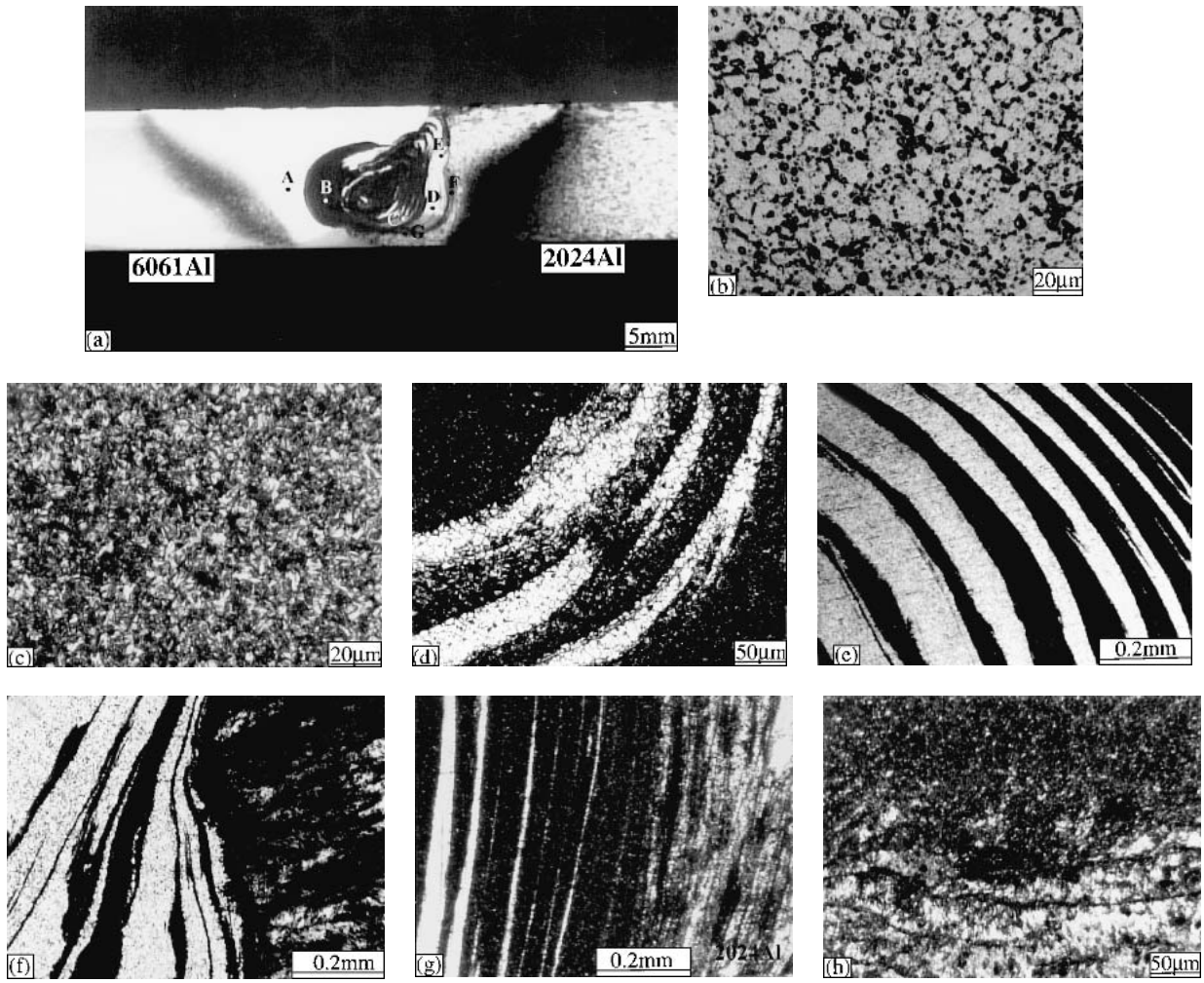

Fig. 5 Typical features of all different zones in a dissimilar weld cross section of 6061-Al to 2024-Al alloy at 637 rpm for rotational speed and 133 mm/min for welding speed: (a) weld cross section (B—B); (b) equiaxed grains of 6061-Al alloy in the UMR of the nugget zone at the position A; (c) microstructure of the MMR in the nugget zone around the position B; (d) micrograph showing the mixing of two Al-alloys around the position C; (e) alternative lamellae of two Al-alloys in the SPFR of the nugget zone around the position D; (f) upper portion of the TMAZ of 2024-Al alloy around the position E; (g) lower portion of the TMAZ of 2024-Al alloy around the position F; (h) deformed 2024-Al alloy around the position G. Positions A–G are marked in (a).

more uniform, and the rotational cell becomes wider and more complete as shown in Fig. 6(d). The width of the mixed region at the beginning of the weld is 15.5 mm, which is much larger than that (7.5 mm) of the mixed region at the steady weld. The thickness of the 6061-Al lamellae in the SPFR at the beginning of the weld is less than 17.0 μm, shown in Fig. 7, which is also much thinner than that (300.0 μm) of the 6061-Al lamellae at the steady weld. At the TMAZ of the 2024-Al alloy side, the deformed grains are parallel to the interface between the nugget zone and TMAZ. As the welding tool advances, the 6061-Al alloy is delivered clockwise around the pin and delivered to different positions in the nugget zone behind the welding tool. Figure 6(f) shows the material flow at the top surface of a dissimilar weld of the 6061-Al to 2024-Al alloy. Although severe plastic deformation is caused by the contact of the tool shoulder, no alternative lamellae of the two alloys is observed on the plan view.

Figure 7 shows the microstructural details of the horizontal section (C—C) at the beginning of a dissimilar weld nugget zone. Distinctly different characteristics of mechanical mixing and material flow at the beginning of the dissimilar welds are observed as contrasted to the steady weld. The flow lines of alternative lamellae are most closely spaced near the interface between the nugget zone and the TMAZ of 2024-Al alloy and become widely separated, depending on the related positions shown in Fig. 7(a). The alternative lamellae of the two Al-alloys near the TMAZ of 6061-Al alloy side are quite irregularly separated as shown in Fig. 7(e). Figure 7(b-d) illustrates the different mixing degree of these two Al-alloys at various positions in the weld nugget. In the MMR near the 2024-Al alloy side, alternative lamellae are not clearly observed except for a large number of discontinuous flow lines of the 6061-Al alloy in the nugget zone shown in Fig. 7(b). Material mixing in Fig. 7(c) is more complete. Dense crushed particles of the two Al-alloys are dispersed into the nugget zone. From Fig. 7(d) near the center of the weld, discontinuous flow lines of thin

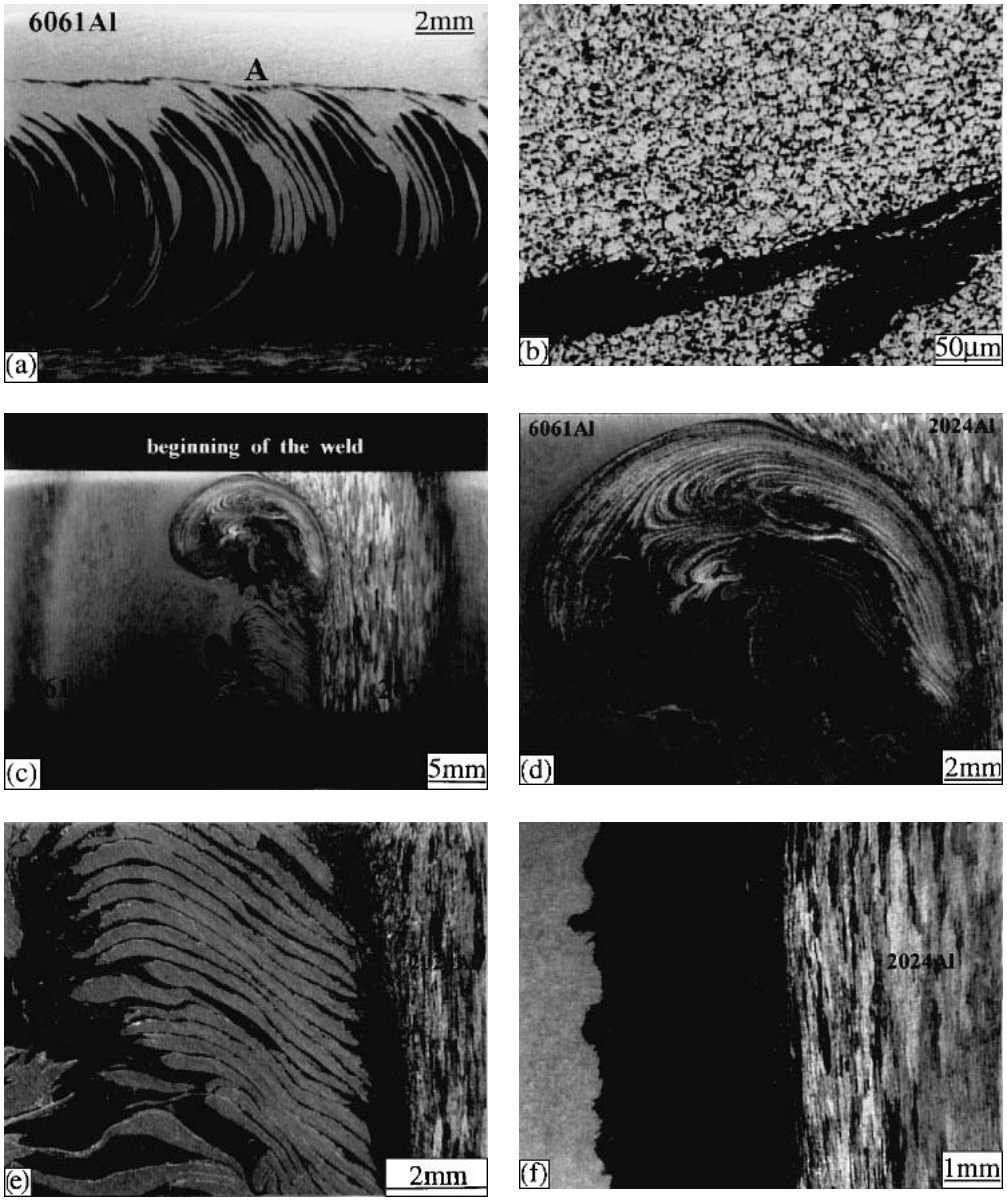

Fig. 6 Typical morphology of longitudinal and horizontal sections of a dissimilar weld of 6061-Al to 2024-Al alloys at 637 rpm for rotational speed and 133 mm/min for welding speed: (a) longitudinal section (A—A) at the centerline; (b) microstructure across the transition interface around the position A marked in (a); (c) horizontal section (C—C) at the mid-thickness of Al-alloy plates, showing distinctly different morphology between the beginning of the weld and the steady weld; (d) high magnification of (c) showing the morphology at the beginning of the weld; (e) high magnification of (c) showing the morphology of the steady weld; (f) plan view at the top surface of a dissimilar weld of 6061-Al to 2024-Al alloys

vortex-like lamellae are observed in the SPFR near the 6061-Al alloy side. The mixing is far from complete despite the repeated stirring action of the threaded tool during the plunge-ment; however, the bonding is clearly finished.

The material flow patterns mostly observed in the nugget zone are very pronounced in dissimilar welds because of the different etching behavior of the 6061-Al alloy (bright regions) and the 2024-Al alloy (dark regions). Mechanical mixing and bonding of material in the nugget zone between the 6061-Al and 2024-Al alloys is shown in Fig. 8. Two mechanisms that allow speculation about how mixing and bonding of material are performed are provided. First, a partial dissolution and dispersion of equiaxed 6061-Al grains along the grain boundaries due to the high temperature appears to produce the dispersed particles of these two Al-alloys in the mechanically mixed layer as shown in Fig. 8(a) and (c). During this process, diffusion of alloy elements along the grain boundaries of the 6061-Al alloy is considered to be dominated. Regions of different compositions are intimately bonded, as evidenced by individual grains growing across the boundaries. Second, the lamellae of two Al-alloys are extruded and crushed by extremely high shear stress and mechanical stirring action in the SPFR as shown in Fig. 8(b) and (d). In this case, mechanical stirring is dominant. Diffusion and mixing of material appears

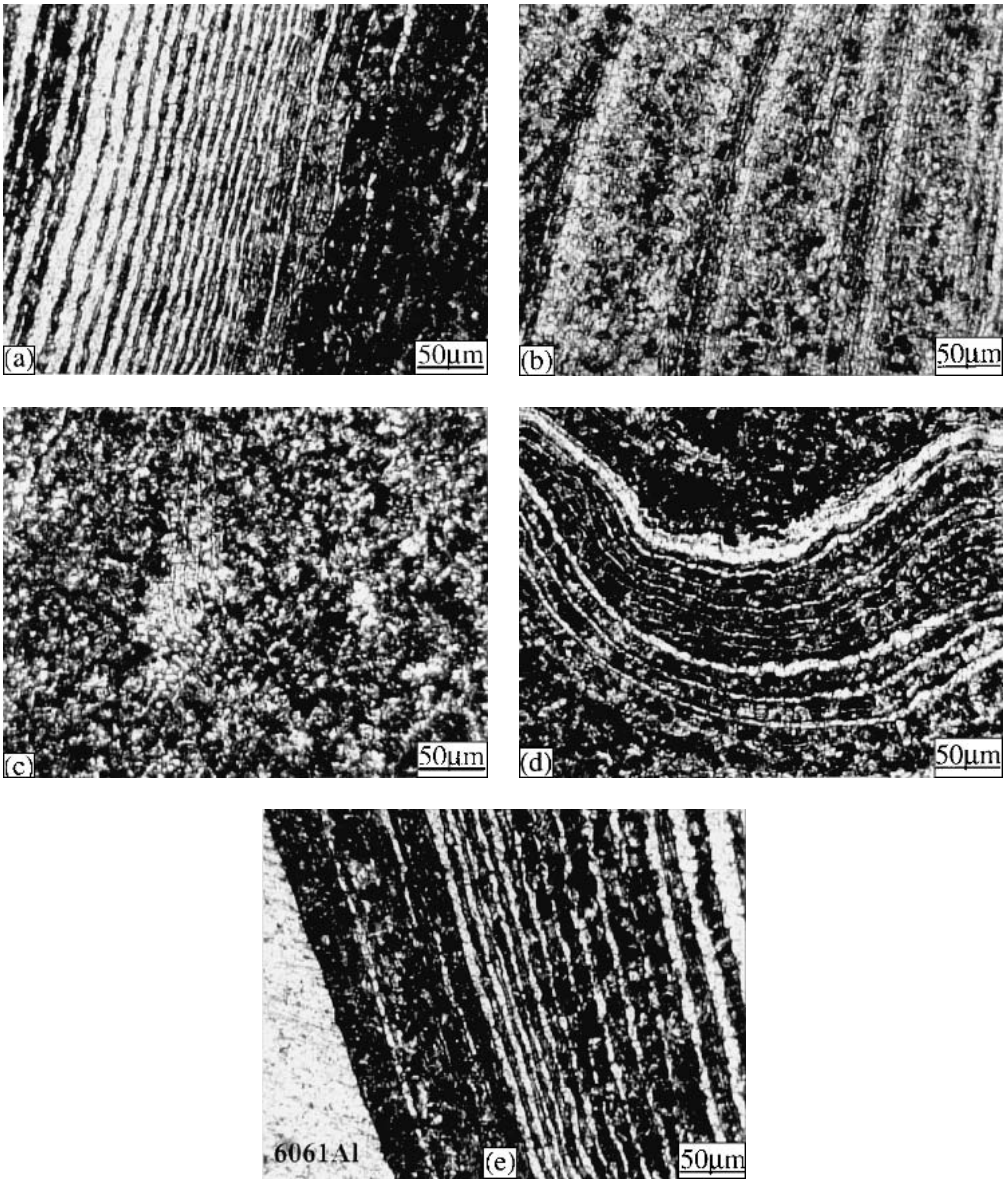

Fig. 7 Microstructural details of the horizontal section (C—C) at the beginning of a dissimilar weld nugget zone: (a) alternative lamellae near the TMAZ of 2024-Al alloy side; (b) mechanically mixed layer; (c) uniformly mixed region; (d) near the center of the dissimilar weld; (e) alternative lamellae near the 6061-Al alloy side

to be limited to a very narrow zone at boundaries. It is worth noting that different indents and hardness value across these interfaces are also caused by these two different mechanisms. The microhardness (97-104 $HV_{0.2}$) of the 6061-Al lamellae shown in Fig. 8(c) is clearly higher than that (75-81 $HV_{0.2}$) of the 6061-Al lamellae shown in Fig. 8(d). These features produce distinct fluctuations of hardness throughout the FSW zone.

Both increasing the rotational speed (Rt) and reducing the welding speed (V) make the material flow stronger. The former, however, had a significantly greater effect. Severe plastic deformation also occurred along the top surface of the weld where the shoulder of the tool was in contact with the workpiece. Herein, the horizontal flow along the shoulder surface shown in Fig. 6(f) is called the surface flow, and the inward flow in the interior of the nugget is called the return flow. Figure 9 shows the effect of the rotational speed on material flow and mechanical mixing in dissimilar welds at the welding speed of 133 mm/min. When the rotational speed is increased from 344 to 637 rpm as shown in Fig. 9 and Fig. 5(a), the return material flow penetrates wider into the 6061-Al alloy side of the nugget zone. At Rt = 344 rpm, material flow is slow and discontinuous across the line of joint. Because the rotational speed is slow, heat resulting from the rotating tool appears not to produce enough high temperature needed for softening the surrounding materials. A lot of weld defects characterized by voids and incomplete root penetration are found at the bottom of the nugget. At Rt = 500 rpm, a larger mechani-

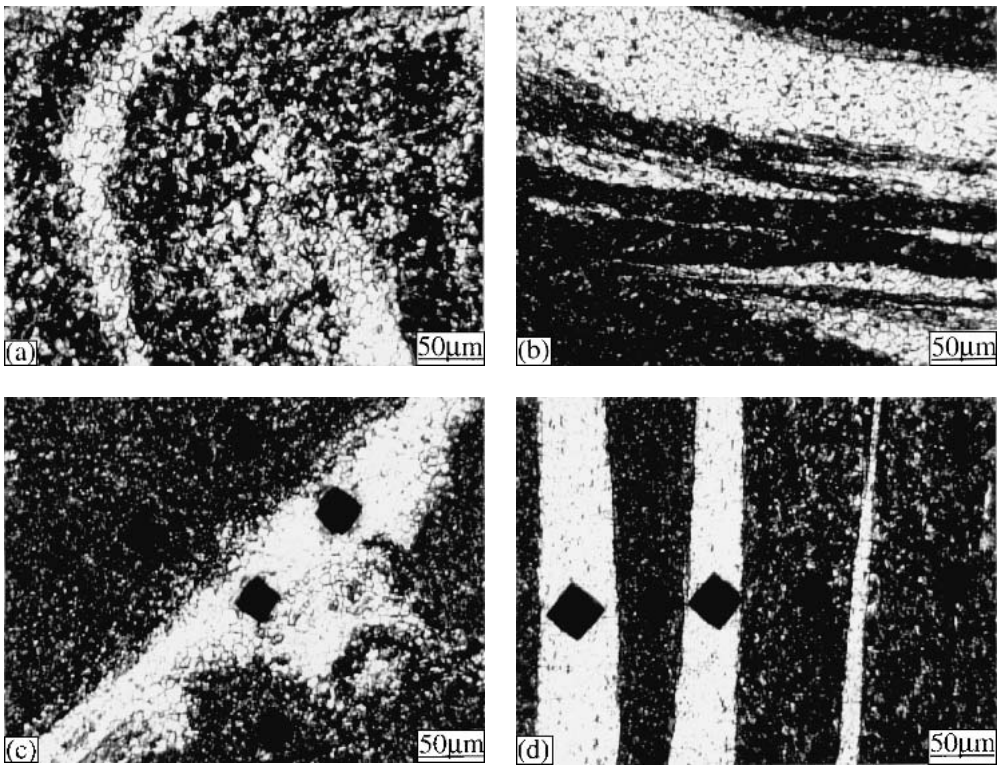

Fig. 8 Mechanical mixing and bonding of material in the nugget zone between 6061-Al and 2024-Al alloys: (a) partial dissolution and dispersion of equiaxed 6061-Al grains along the grain boundaries; (b) interface caused by shear stress and mechanical stirring action; (c) indents in the mixed region of different alloy constituents; (d) indents in the alternative lamellae caused by the threaded tool

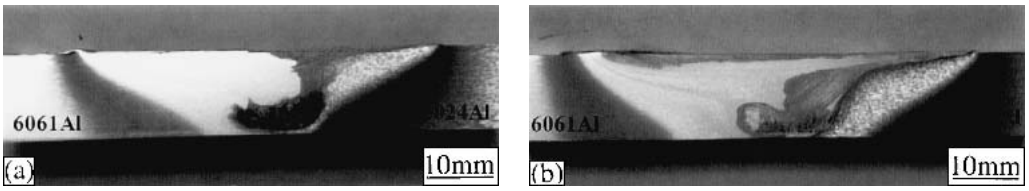

Fig. 9 Effect of the rotational speed on material flow and mechanical mixing in a dissimilar weld of 6061-Al to 2024-Al alloys at welding speed of 133 mm/min: (a) Rt = 344 rpm; (b) Rt = 500 rpm

cally mixed layer is found in the nugget zone. A somewhat alternative lamellae of two Al-alloys is evidenced by more material flow at the 2024-Al alloy side as shown in Fig. 9(b). Only a small amount of voids is detected at the bottom of the nugget. At Rt = 637 rpm, the material flow is significantly faster, the clockwise rotating cell is observed in the nugget zone in Fig. 5(a). However, the cell, in fact, looks more triangular than round. Because the rotational speed is higher now, the return flow also has to be faster to satisfy the continuity requirement. This requirement gives the return flow more momentum to penetrate wider and mix more uniformly, even though this means the return flow has to travel a longer distance and at a higher velocity into the center of the nugget.

Figure 10 shows the effect of the welding speed on the material flow and mechanical mixing in the dissimilar 6061-Al/2024-Al welds at rotational speed of 637 rpm. The flow patterns are revealed clearly by flow visualization of the cross-sectional examinations. At V = 57 mm/min, the mechanical mixing becomes more uniform, and the cells become rounder and more complete as contrasted to V = 133 mm/min in Fig. 5 (a). Cross-sectional examinations as shown in Fig. 10(a) and (c) reveal a vortex-like clockwise rotating cell structure. The material flow is steady and asymmetric. When the welding speed is increased to 229 mm/min, there is a very distinct secondary cell at the subsurface of the dissimilar metal weld as shown in Fig. 10(b) and (d). Two clockwise rotating cells consisting of the alternative lamellae of the two Al-alloys are observed at the weld crosssection. The faster welding speed requires a faster return flow to satisfy continuity, and the return flow takes a shortcut back to the surface instead of reaching the root of the nugget. This may result in two or multiple rotating cells. The alternative lamellae structure in the SPFR is clearly evident because of the stirring action of the threaded tool. However, the thickness and deformation degree of the 6061-Al lamellae mainly depends on the welding parameters. From Fig. 10(d), the thick 6061-Al lamellae are stirred, in situ extruded,

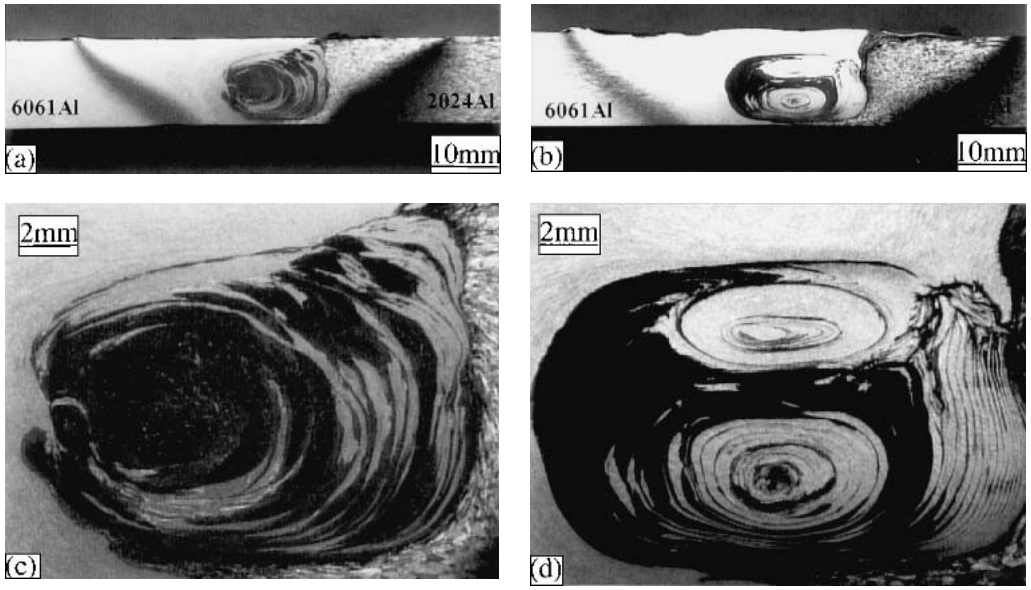

Fig. 10 Effect of the welding speed on material flow and mechanical mixing in a dissimilar weld of 6061-Al to 2024-Al alloys at rotational speed of 637 rpm: (a) 57 mm/min; (b) 229 mm/min; (c) high magnification of (a); (d) high magnification of (b)

and pulled under the extreme shear stress along the surface of the tool thread from one side to another side and then deposited at the center. The material at the 6061 Al-alloy side flows inward along the weld surface, turns downward at the surface of the tool at the 2024 Al-alloy side to fall along the thread line, and then returns to the center of the nugget. The centers of the cells are close to the 2024 Al-alloy side. From Fig. 10(d), it appears the maximum velocity of material flow is at the bottom of the nugget, and the return flow at the lower region is much stronger than that at the upper region.

Figure 11 shows the AE signals recorded at both the 6061-Al and the 2024-Al alloy sides of the joint at 637 rpm for the rotational speed, and 133 mm/min for the welding speed. The peak amplitudes of the AE signals are quite different from those obtained in the welds of the 6061-Al alloy to itself as shown in Fig. 4. The sensor placed at the 2024-Al alloy side only detects a slightly stronger AE signal than that placed at the 6061-Al alloy side. Figure 11(c) shows the processed AE signals generated by the plastic deformation and flow of material during the FSW of the 6061-Al to 2024-Al alloy. This result indicates that only slightly more plastic deformation and material flow appears at the 2024-Al alloy side, which is much different from Fig. 4. The difference of AE signals in Fig. 4 and 11 may be explained by the higher yield strength and resistance to the plastic deformation of the 2024-Al alloy than those of the 6061-Al alloy.

3.3 Microhardness Distribution in the Same and Dissimilar Metal Welds

Figure 12(a) shows the typical microhardness distribution of cross sections in the same and dissimilar metal welds of the 6061-Al alloy to itself, and 6061-Al alloy to 2024-Al alloy. In the weld of the 6061-Al alloy to itself, the minimum hardness values (55-65$HV_{0.2}$) are obtained near the HAZ/TMAZ interface, and there is an increase in hardness across the TMAZ (65-70$HV_{0.2}$) and weld nugget (75-85$HV_{0.2}$) that is generally less than that of the parent metal of 6061-Al alloy as shown in Fig. 12(a). The hardness of the unaffected parent metal is in the range of 90-100 $HV_{0.2}$ for the 6061-T6 Al-alloy and 130-140 $HV_{0.2}$ for the 2024-T3 Al-alloy. A significant variation in hardness as shown in Fig. 12(a) is found across the dissimilar welds. The minimum value is about 60$HV_{0.2}$ in the HAZ on the 6061-Al alloy side. The hardness at the TMAZ and the UMR of the nugget zone at the 6061-Al alloy side are 65-70$HV_{0.2}$ and 75-80$HV_{0.2}$, respectively. There is a fluctuating hardness (75-145$HV_{0.2}$) in the SPFR of the nugget zone that is related to the alternative lamellae of the two Al-alloys. The maximum hardness is typically 130-150 $HV_{0.2}$ in the MMR of the nugget zone, in which the relatively uniform mixing of two Al-alloys is reached. No distinct variations in hardness are found in both the TMAZ (130-140 $HV_{0.2}$) and HAZ (125-135 $HV_{0.2}$) of the 2024-Al alloy side as contrasted to the parent metal (130-140 $HV_{0.2}$) of the 2024 Al-alloy.

Figure 12(b) shows the typical microhardness distribution along the longitudinal sections in the same and dissimilar metal welds. It can be seen that the hardness in the weld nugget of 6061-Al to itself is almost the same. However, different levels of hardness are obtained for the dissimilar weld nugget as shown in Fig. 12 (b). The hardness variations are related to different Al-alloys. The hardness, tensile strength, and elongation of the 2024-T3 Al-alloy (120-130 $HV_{0.2}$, 485 Mpa, and 18%) are distinctly higher than those of the 6061-T6 Al-alloy (90-100 $HV_{0.2}$, 310 Mpa, and 12%). As expected, the TMAZ and HAZ at the 6061 Al-alloy side are considerably softened in contrast with those at the 2024 Al-alloy side as shown in Fig. 12 (a). As can be seen by comparing the microstructure and measured hardness, there is a good correlation between the hardness and distribution of the two different Al-alloys caused by the material flow.

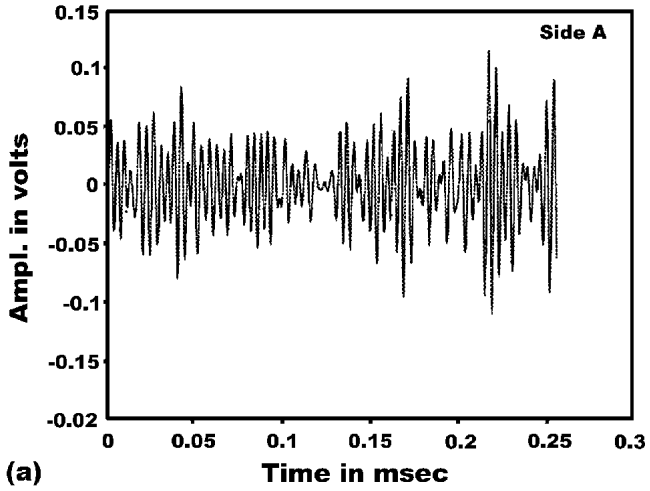

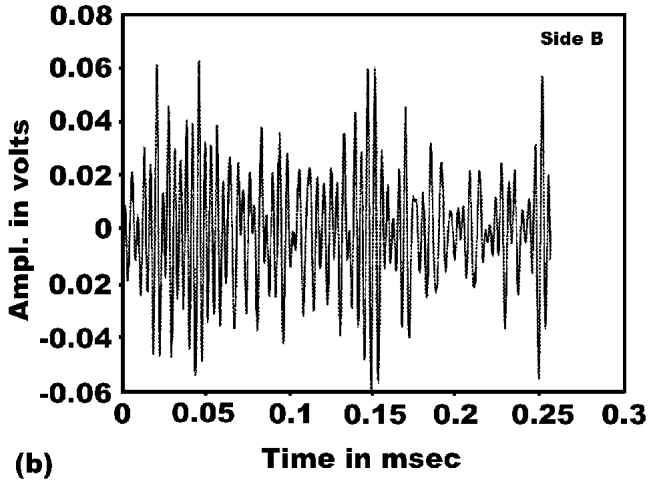

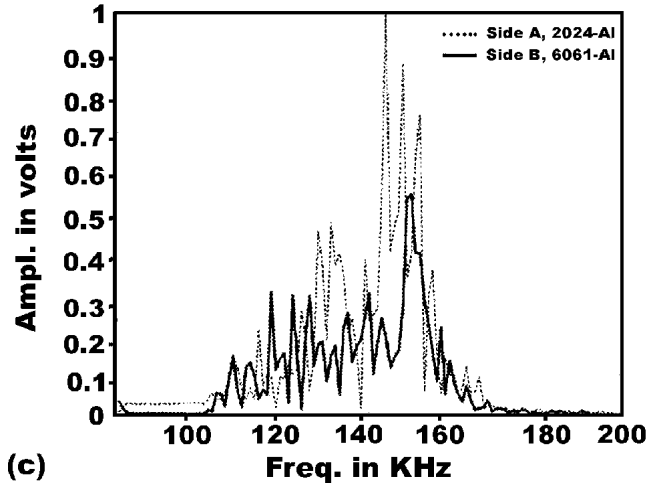

Fig. 11 Acoustic emission (AE) signals recorded at both sides of a dissimilar weld of 6061-Al to 2024-Al alloys at 637 rpm for rotational speed, and 133 mm/min for welding speed: (a) typical AE signals at the 2024-Al alloy side; (b) typical AE signals at the 6061-Al alloy side; (c) processed AE signals at both sides of the weld

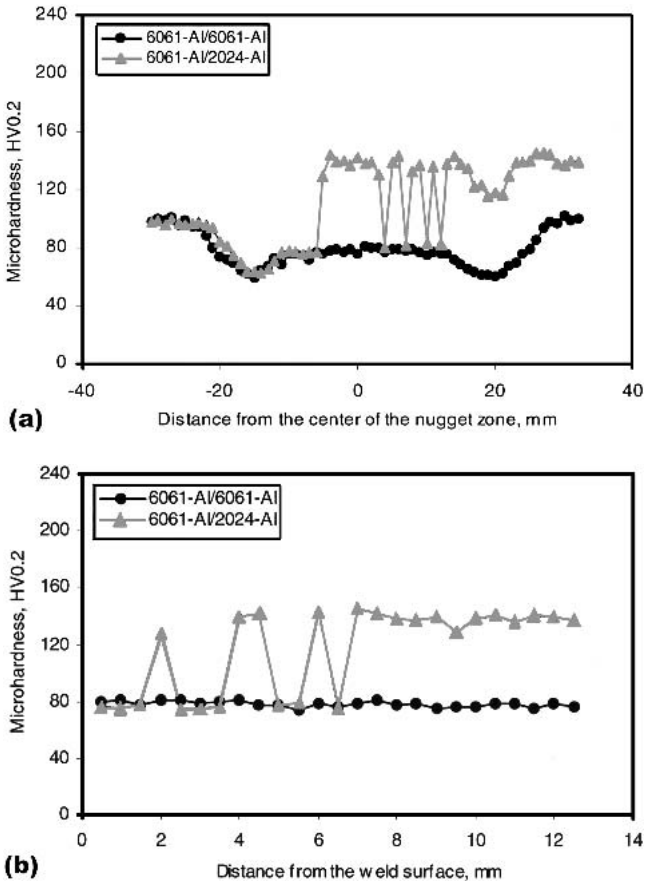

Fig. 12 Typical microhardness distributions in the same and dissimilar metal welds of 6061-Al alloy to itself, and 6061-Al to 2024-Al alloys (the welding parameters are 416 rpm and 133 mm/min for the same metal weld, and 637 rpm and 133 mm/min for the dissimilar metal weld, respectively): (a) cross sections; (b) longitudinal sections

4. Conclusions

From the performed analyses the following conclusions can be derived:

- Plastic deformation, flow, and mechanical mixing of material exhibit distinctly asymmetric characteristics at both sides of the same and dissimilar welds.
- The microstructure in a dissimilar 6061-Al/2024-Al weld is distinctly different from that in a weld of the 6061-Al alloy to itself. A vortex-like structure featured by concentric flow lines for the 6061-Al alloy to itself, and alternative lamellae with different alloy constituents for the 6061-Al alloy to 2024-Al alloy is attributed to the stirring action of the threaded tool, in situ extrusion, and traverse motion along the welding direction. The mutual mixing in a dissimilar 6061-Al/2024-Al weld is intimate and far from complete. However, the bonding between the two alloys is clearly complete.
- Three different regions in the nugget zone of the dissimilar 6061-Al/2024-Al weld are classified by the MMR characterized by the dispersed particles of different alloy con-

stituents, the SPFR featured by the alternative lamellae of the two Al-alloys, and the UMR consisting of fine equiaxed grains of the 6061-Al alloy. Within all of these three regions, the material is able to withstand the very high degree of plastic deformation due to the presence of a dynamic recovery and recrystallization of the microstructure. The degree of material mixing, the thickness of the deformed Al-alloy lamellae, and the material flow patterns depend on the related positions in the nugget zone, and the processing conditions. These features produce distinct fluctuations of hardness throughout the weld.

- The width and shape of the nugget zone in the dissimilar metal weld is greatly associated with the welding parameters. As the rotational speed becomes faster, the mechanical mixing of the material in the dissimilar welds becomes more uniform, and the single or multiple cells of the material flow with the alternative lamellae of different alloy constituents becomes rounder and more complete. A higher rotational speed gives the return flow of the material more momentum to penetrate wider and mix more uniformly, even though this means the return flow has to travel a longer distance and at a higher velocity into the center of the nugget.

Acknowledgments

This work was financially supported by the U.S. Department of Education, Grant No. P200A80806-98, by the Brown Foundation, Houston, TX, and by SMU. The authors also are grateful for the technical support of Mr. Valant, Mr. Song, and Mrs. Jandric.

References

1. W.M. Thomas, E.D. Nicholas, J.C. Needham, M.G. Murch, P. Templesmith, and C.J. Dawes: "Friction Stir Welding Butt Welding," G.B. Patent Application No. 9125978.8, Dec. 1991; U.S. Patent No. 5460317, Oct. 1995.
2. K. Colligan: "Material Flow Behavior during Friction Stir Welding of Aluminum," *Weld. J., 75*(7), 1999, pp. 229s-37s.
3. H. Larsson, L. Karlsson, S. Stoltz, and E.L. Bergqvist: "Joining of Dissimilar Al-alloys by Friction Stir Welding," *2nd International Symposium on Friction Stir Welding,* 26-28 June 2000.
4. T. Hashimoto, N. Nishikawa, S. Tazaki, and M. Enomoto: "Mechanical Properties of Joints for Aluminum Alloys with Friction Stir Welding Process," in *Proc. Conf. INALCO'98, 7th International Conference Joints in Aluminum,* April 1998, TWI.
5. F. Palm: "Charakterisierung des Materialflusses beim Reibruehrschweissen (Friction Stir Welding) von Al-Werkstoffen," in Proc. GKSS/TWI Workshop on "Friction Stir Welding", May 1999, pp. 23-29.
6. P. Threadgill: "Friction Stir Welds in Aluminum Alloys—Preliminary Microstructural Assessment," *TWI Bulletin,* 1997, *38*(2), pp. 30-33.
7. C.G. Rhodes, M.W. Mahoney, and W.H. Bingel: "Effects of Friction Stir Welding on Microstructure of 7075 Aluminum," *Scr. Mater.,* 1997, *36*(1), pp. 69-75.
8. E.D. Nicholas and S.W. Kallee: "Friction Stir Welding—A Decade On," *IIW Asian Pacific International Congress,* Sydney, 29 October to 2 November 2000, pp. 1-12.
9. W.M. Thomas: "Friction Stir Welding of Ferrous Materials—a Feasibility Study," *1st International Symposium on Friction Stir Welding,* 14-16 June 1999.
10. L.E. Murr, G. Liu, and J.C. McClure: "A TEM Study of Precipitation and Related Microstructures in Friction-Stir-Welded 6061 Aluminum," *J. Mater. Sci.,* 1998, *33,* pp. 1243-51.
11. A.P. Reynolds, W.D. Lockwood, and T.U. Seidel: "Processing-Property Correlation in Friction Stir Welds," *Mater. Sci. Forum,* 2000, *331-337,* pp. 1719-24.
12. P. Colegrove: 3-Dimensional Flow and Thermal Modeling of the Friction Stir Welding Process, *2nd International Symposium on Friction Stir Welding,* 26-28 June 2000.
13. C.B. Smith, G.J. Bendzsak, T.H. North, J.H. Hinrichs, J.S. Noruk, and R.J. Heideman: "Heat and Material Flow Modeling of the Friction Stir Welding Process," *2nd International Symposium on Friction Stir Welding,* 26-28 June 2000.
14. Y. Li, L.E. Murr, and J.C. McClure: "Solid-State Flow Visualization in the Friction-Stir Welding of 2024 Al to 6061 Al," *Scr. Mater.,* 1999, *40*(9), pp. 1041-46.
15. L.E. Murr, Y. Li, E.A. Trillo, R.D. Flores, and J.C. McClure: "Microstructures in Friction-Stir Welded Metals," *J. Mater. Process. Manuf. Sci.,* 1998, *7*(10), pp. 145-61.
16. L.E. Murr, Y. Li, R.D. Flores, E.A. Trillo, and J.C. McClure: "Intercalation Vortices and Related Microstructural Features in the Friction-Stir-Welding of Dissimilar Metals," *Mater. Res. Innovat.* 1998, *2,* pp. 150-63.
17. Y. Li, E.A. Trillo, and L.E. Murr: Friction-Stir Welding of Aluminum Alloy 2024 to Silver, *J. Mater. Sci. Lett.,* 2000, *19,* pp. 1047-51.
18. L.E. Murr, R.D. Flores, O.V. Flores, J.C. McClure, G. Liu, and D. Brown: "Friction-Stir Welding: Microstructural Characterization," *Mater. Res. Innovat.,* 1998, *1,* pp. 211-23.
19. L.E. Murr, Ying Li, E.A. Trillo, and J.C. McClure: "Fundamental Issues and Industrial Applications of Friction-Stir Welding," *Mater. Technol.,* 2000, *15*(1), pp. 37-48.